PAPER

Check for updates

Enhanced proton conductivity from phytic acid-intercalated three-dimensional graphene oxide†

Shakiba Salehpour,[a] Lutfia Isna Ardhayanti, [iD][a] Yoshiharu Hidaka,[a] Xinyao Liu,[a] Tatsuki Tsugawa,[b] Kazuto Hatakeyama, [iD][c] Md. Saidul Islam, [iD]*[a] Yoshihiro Sekine, [iD][ad] Shintaro Ida [iD][bc] and Shinya Hayami [iD]*[ace]

Despite graphene oxide (GO) and its derivatives showing potential as a proton conductor, the practical implications of GO-based membranes require further optimization of their proton conductivity. Herein, we report the improved proton-conducting properties of phytic acid intercalated three-dimensional graphene oxide (Phy-3DGO). The Phy-3DGO was prepared using a freeze-drying process. Experimental results prove enhanced proton conductivity with a magnitude of 2.45×10^{-1} S cm^{-1} at 65 °C and 90% RH in the out-of-plane direction compared to 3.21×10^{-3} S cm^{-1} for 3DGO under similar experimental conditions. The low activation energy value of 0.26 eV for Phy-3DGO indicates the proton conduction through the Grotthuss mechanism. In the single-cell performance test, a maximum current density of 1210 mA cm^{-2} and a maximum power density (MPD) of 248.2 mW cm^{-2} were achieved using a 170 μm-thick Phy-3DGO film, compared to an MPD of 98.1 mW cm^{-2} for 3DGO. These findings highlight the synergistic effects of graphene oxide and phytic acid in improving the interlayer distance and water retention, resulting in improved proton transport pathways. The study offers valuable insights into developing sustainable and efficient energy storage systems.

Introduction

In the past decades, graphene oxide (GO) has drawn significant attention due to its exceptional physical and chemical properties, including high mechanical strength, excellent thermal and electrical conductivities, and a large surface area. These attributes make GO a highly versatile material with potential applications across various fields, particularly in energy storage and conversion systems.[1–6] One of the intriguing features of GO is its abundance of oxygenated functional groups, such as hydroxyl, epoxy, and carboxyl groups that extend from the hydro-phobic carbon skeleton.[7] Under humidified conditions, these hydrophilic sites can adsorb water molecules that function as the vehicle

for the movement of the proton *via* a Grotthuss mechanism, making it a promising candidate for high proton conductivity applications.[8–10] However, the proton-conducting properties of GO are not adequate for practical use and require optimization using an appropriate strategy.

The proton exchange membrane (PEM) showing adequate proton conduction is a critical parameter in the overall performance of proton exchange membrane fuel cells (PEMFCs), which are considered one of the most promising and environmentally friendly technologies for converting chemical energy into electrical energy.[11,12] Traditional PEM materials, such as Nafion, along with a high proton conductivity of $\sim 10^{-4}$–10^{-2} S cm^{-1}, have set a high benchmark for performance as proton exchange membranes. However, the high cost related to the synthesis of Nafion, environmental toxicity, and limited stability in operating under harsh conditions largely limit the wide commercialization of its use in fuel cell applications.[13,14] Consequently, there is an ongoing quest to develop alternative materials that can offer comparable or superior properties at a lower cost and with enhanced environmental compatibility. In this context, the modification of GO to enhance its proton conductivity has emerged as a promising research direction. In addition to high proton conductivity, GO-based membranes also facilitate physicochemical stability, abundance, and nontoxic nature.

[a] Department of Chemistry, Graduate School of Science and Technology, Kumamoto University, 2-39-1 Kurokami, Chuo-ku, Kumamoto 860-8555, Japan. E-mail: hayami@kumamoto-u.ac.jp

[b] Faculty of Engineering, Graduate School of Science and Technology, Kumamoto University, 2-39-1 Kurokami, Chuo-ku, Kumamoto 860-8555, Japan

[c] Institute of Industrial Nanomaterials (IINa), Kumamoto University, 2-39-1 Kurokami, Chuo-ku, Kumamoto 860-8555, Japan

[d] Priority Organization for Innovation and Excellence, Kumamoto University, 2-39-1 Kurokami, Chuo-ku, Kumamoto 860-8555, Japan

[e] International Research Center for Agricultural and Environmental Biology (IRCAEB), 2-39-1 Kurokami, Chuo-ku, Kumamoto 860-8555, Japan
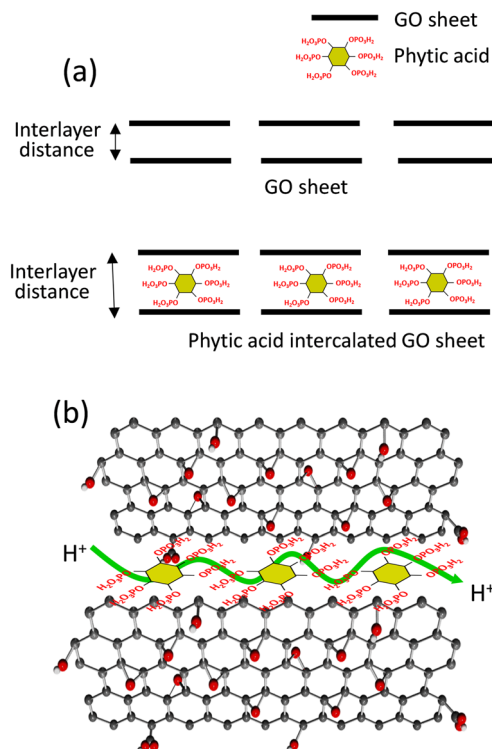
† Electronic supplementary information (ESI) available. See DOI: https://doi.org/10.1039/d4lf00364k

Before the discovery of GO as a single-phase proton conductor, GO materials were attempted as additives in traditional proton conducting membranes, including Nafion, to improve conductive properties and stability.[15–17] Our group reported the significant in-plane proton conductivity of a single-layer GO nanosheet using a comb-shaped microelectrode for the first time.[18] Moreover, we identify the mechanism of proton conduction while we find that the epoxy groups are majorly responsible for the high proton conductivity of GO nanosheets.[19] After that, several strategies, including multilayer stacking, increasing the oxygen content by ozonation, and intercalating different hydrophilic groups/ions onto the GO-walled channels have been applied to improve the proton conductivity of GO-based materials.[20–26] The enhanced GO-based proton conduction has been attributed to some crucial factors, including the increase in the interlayer distance between the GO layers, hence in the hydrophilic functional groups and the water uptake ability.[26]

Despite the high in-plane proton conductivity of GO, poor single-cell performance has been reported for the vacuum-filtration-induced GO membrane when employed as the electrolyte. This is likely a consequence of poor proton transfer in the out-of-plane direction with respect to the GO membrane under operating conditions. As a possible solution, our research group reported the structural transformation of GO into the three-dimensional GO (3DGO) without destroying the hydrophilic functional groups, resulting in significantly high proton conduction in the out-of-plane direction.[27] A 3D interconnected network with significant interlayer void space and high internal surface area is found to promote water uptake and facilitate facile proton conduction track formation.

Nevertheless, the proton conductivity and device performance of the 3DGO are not enough for practical application, and cell performance should be further improved to obtain the high-power density PEMFC. The optimization in the proton conduction in 3DGO might be the key route. Among various modification strategies, intercalation with hydrophilic functional sites that can adjust with GO and participate in improving the interlayer distance and water absorption ability is very effective. In this contest, herein we use phytic acid as a potential candidate. Phytic acid, a naturally occurring substance found in plant seeds, is rich in phosphate groups. In particular, six phosphoric acid groups are attached in the six corners of cyclohexene. When used to modify GO, phytic acid can introduce additional functional groups and create an interconnected three-dimensional structure that facilitates proton conduction. This phytic acid-modified 3D graphene oxide (Phy-3DGO) framework is expected to retain the inherent advantages of GO, and the addition of phytic acid can enhance the interlayer distance in the resultant Phy-3DGO (Scheme 1a). Furthermore, introducing phytic acid is hypothesized to enhance the water adsorption capacity and create a continuous network of hydrogen-bonded pathways, which

Scheme 1 Phytic acid intercalated graphene oxide. a) Improvement in the interlayer distance due to the intercalation of phytic acid in GO and b) an expected better hydration pathway for improved proton conductivity in the phytic acid intercalated 3DGO.

can significantly boost proton transport under humid conditions (Scheme 1b).

Experimental

All reagents used in this study were of analytical grade and utilized without further purification.

GO was obtained from NSC Co. Ltd., and the concentration of GO dispersion was maintained at 0.5 mg mL^{-1} using the appropriate amount of water. The 3DGO was prepared using a freeze-drying method described in our previous report.[27] Phytic acid-modified GO was synthesized by incorporating an appropriate amount of phytic acid into the GO while maintaining a GO : phytic acid ratio of : 1 (weight ratio), followed by stirring for 2 h and drying using a freeze-dry route. For proton conductivity measurements, 3DGO and Phy-3DGO membrane samples were prepared by applying a pressure of 10 Mpa.

The morphological and structural characteristics of the samples were characterized using field emission scanning electron microscopy (FE-SEM, JSM-7600F, JEOL), Fourier transform infrared (FT-IR) spectroscopy (Spectrum Two, PerkinElmer), Raman spectroscopy (NRS-3100, JASCO), and Thermogravimetry (TGA, TG/DTA 6300, Seiko Instruments, Inc.).

Proton conductivities were measured using the alternating current (AC) impedance method with an impedance/gain

phase analyzer (MTZ-35, Bio-Logic Science Instruments) over a frequency range of 1 Hz to 1 MHz. The temperature and humidity of the system were controlled using an incubator (IW223, Yamato Scientific Co.).

Proton conductivity in both the in-plane and out-of-plane directions was measured. In the case of in-plane direction proton conductivity measurement, two platinum wires were placed on the same side of the membrane. Proton conductivity (σ) was calculated using the formula $\sigma = d/LTR$, where R is the measured resistance, T is the thickness of the membrane, d is the distance between the electrodes, and L is the length of the sample that is perpendicular to d.

On the other hand, to measure out-of-plane conductivity, a membrane of each sample was prepared with both sides coated in gold paste and attached to gold wires (50 μm diameter, Tanaka Kikinzoku Kogyo K. K.) to form the measurement cell. Proton conductivity (σ) was calculated using the formula $\sigma = d/SR$, where S is the electrode area, R is the measured resistance, and d is the thickness (distance between the electrodes).

Results and discussion

Fig. 1 and S1† present the morphological and chemical properties of 3DGO and Phy-3DGO. Fig. S1† shows the optical images of 3DGO and Phy-3DGO. A little change in the sample color is observed due to the addition of phytic acid in the GO. The SEM images in Fig. 1a and b provide a more detailed look at the surface morphology of 3DGO and Phy-3DGO. A notable difference between these two samples is the decreased aggregation and enhanced dispersion in Phy-3DGO, likely due to the intercalation of phytic acid. The inclusion of phytic acid disrupts the restacking of GO sheets, resulting in a more homogeneous and open structure. The cross-sectional SEM image of Phy-3DGO in Fig. 1c reveals a traditional layered structure with a defined layer-by-layer arrangement. This indicates that phytic acid does not disrupt the basic layered architecture of GO but instead alters the interlayer spacing and interaction between layers.

The changes in the interlayer distance were quantitatively evaluated using PXRD analysis, as shown in Fig. 1d. The 3DGO exhibited a peak at 8.97°, corresponding to an interlayer distance of 1.02 nm. In contrast, the Phy-3DGO sample showed a broad peak around 7°, indicating a larger interlayer distance of 1.26 nm. This significant increase in interlayer spacing is attributed to the introduction of bulky phosphate groups from phytic acid, which intercalate between the GO layers. The increased spacing is expected to allow for better ion transport and higher water retention, as the larger void spaces can hold more water molecules,
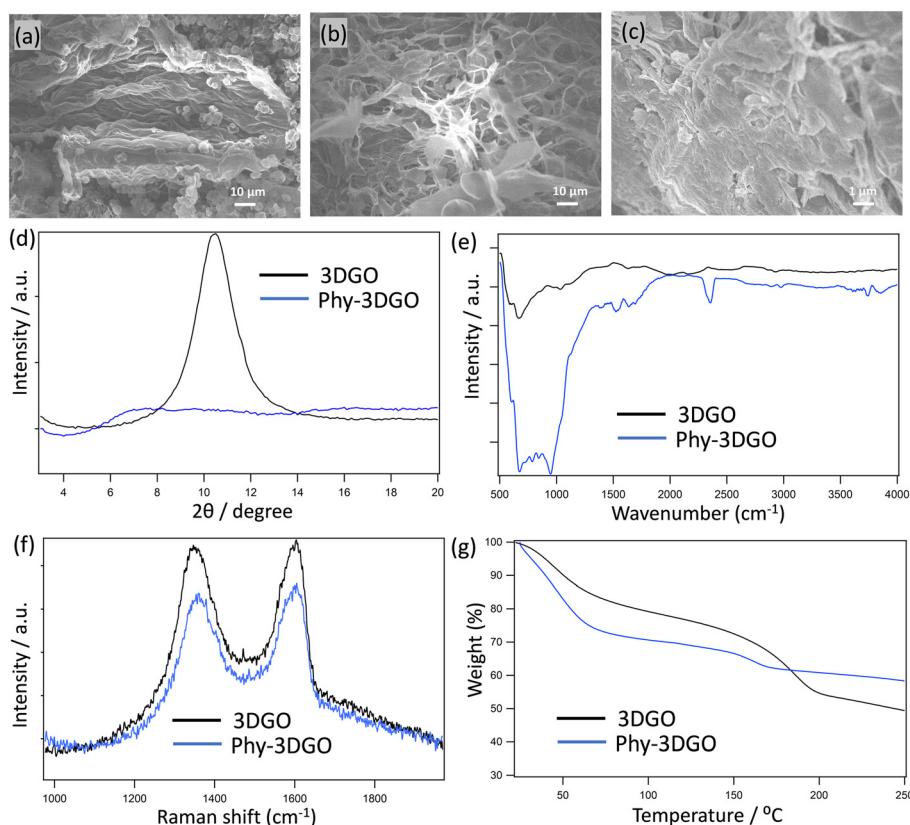

Fig. 1 Morphological and chemical properties of 3DGO and Phy-3DGO. a) SEM image of 3DGO, b) SEM image of Phy-3DGO, c) cross-sectional SEM image of Phy-3DGO, d) PXRD of 3DGO and Phy-3DGO, e) FTIR of 3DGO and Phy-3DGO, f) Raman spectra of 3DGO and Phy-3DGO and g) TGA analysis of 3DGO and Phy-3DGO.

RSC Applied Interfaces

Paper

especially under humid conditions. 3DGO exhibits a sharp PXRD peak, corresponding to the well-ordered stacking of its layers. However, upon mixing with phytic acid, this peak becomes significantly broader compared to other intercalated materials, such as sulfate ions.[28] The pronounced broadening arises from the unique characteristics of phytic acid, which is a bulky, multi-branched molecule with six phosphate groups. Its large size and complex structure introduce substantial steric hindrance and disrupt the regular stacking order of GO layers. Additionally, the multiple functional groups of phytic acid form extensive hydrogen bonds and electrostatic interactions with oxygen-containing groups of GO, leading to a highly disordered and irregular interlayer arrangement. This results in variable interlayer spacing, further contributing to the peak broadening. In contrast, smaller ions like sulfate induce less disruption due to their simpler structure and lower steric effects, resulting in comparatively sharper PXRD peaks.[28]

In addition, to confirm the distribution of phytic acid in Phy-3DGO, we performed an XPS study on the surface of the materials and on the inside part. The elemental percentages are shown in Table S1.† The functional groups on the inside and surface of Phy-3DGO do not differ significantly, ensuring the distribution of phytic acid in the whole GO. Compared to pristine 3DGO, the oxygen content increased by approximately 11%, along with the addition of about 8% phosphorus. These changes enhance water retention, which subsequently facilitates efficient proton conduction.

The FTIR spectra of 3DGO and Phy-3DGO (Fig. 1e) provide further confirmation of the chemical modification introduced by phytic acid. The 3DGO sample shows characteristic peaks associated with oxygen-containing functional groups, consistent with the previous reports.[20] In Phy-3DGO, however, a new peak at 980 cm^{-1} appears, confirming the presence of phosphate groups.[29] This indicates the successful incorporation of phytic acid into the GO structure, modifying the surface chemistry while preserving the overall GO framework.

Raman spectra (Fig. 1f) of both 3DGO and Phy-3DGO exhibit the characteristic D and G bands of GO, without significant shifts in the peak positions or intensity. This suggests that the addition of phytic acid does not introduce significant structural defects in the GO layers. The preservation of the GO framework ensures that the electronic properties of the material remain largely intact while benefiting from the enhanced proton transport introduced by phytic acid. The TGA curves (temperature gradient 5 °C min^{-1}) in Fig. 1g show the water adsorption properties of 3DGO and Phy-3DGO after exposure to 90% relative humidity (RH) for 1 hour. Both materials show weight loss due to water evaporation up to 100 °C, but Phy-3DGO exhibits a significantly higher weight loss of 26.3%, compared to 18.4% for 3DGO. This indicates that Phy-3DGO retains more water, likely due to its increased functional groups (Table S1†) and enhanced interlayer spacing (Fig. 1d). The additional void space created by the phosphate group intercalation allows for

higher water molecule adsorption, which is crucial for maintaining high proton conductivity in humid environments. The ability of Phy-3DGO to absorb and retain more water under high humidity conditions directly correlates with its enhanced proton conduction properties.

The proton conductivity of both 3DGO and Phy-3DGO was investigated in both the in-plane and out-of-plane directions as a function of relative humidity (RH) at room temperature and temperature at 90% RH. The representative Nyquist plot for Phy-3DGO in the out-of-plane direction at 25 °C under 90% RH, as shown in Fig. S2,† indicates that the traces of the real (Z') and imaginary (Z'') parts of impedance fit distorted semicircular curves. The radius of these semicircular curves represents the resistance in proton conduction. The proton conductivity was then calculated based on the equation described in the experimental section. These results are shown in Fig. 2. In the in-plane direction (Fig. 2a), the proton conductivity of both 3DGO and Phy-3DGO increased steadily with rising humidity. At 40% RH, the in-plane proton conductivity of 3DGO was measured at 1.4×10^{-4} S cm^{-1}, while Phy-3DGO showed a significantly higher conductivity of 7.3×10^{-3} S cm^{-1}. As the RH increased to 90%, the conductivity for 3DGO rose to 1.11×10^{-2} S cm^{-1}, whereas that for Phy-3DGO reached 1.07×10^{-1} S cm^{-1}. Compared to pristine 3DGO, the significant improvement in the proton conductivity of Phy-3DGO under the same humidity conditions is due to the intercalation of phytic acid. Phytic acid introduces additional oxygen and phosphate groups, which enhance water retention. This improved hydration is crucial for maintaining high proton conductivity under humid conditions. Fig. 2b presents the temperature-dependent proton conductivity at 90% RH. For both 3DGO and Phy-3DGO, the proton conductivity increased with increasing temperature, as expected for proton-conducting materials. As the temperature increased to 65 °C, the conductivity of 3DGO increased to 0.19 S cm^{-1}, while that of Phy-3DGO reached 0.72 S cm^{-1}. This indicates that Phy-3DGO maintains superior conductivity across the temperature range, likely due to the increased water retention and proton-conducting phosphate groups provided by the phytic acid modification.

The out-of-plane proton conductivity as a function of RH and temperature is presented in Fig. 2c and d, respectively. At 40% RH and 25 °C (Fig. 2c), the out-of-plane conductivity of 3DGO was relatively low at 3.94×10^{-7} S cm^{-1}, increasing to 2.23×10^{-4} S cm^{-1} at 90% RH. In contrast, Phy-3DGO showed a much higher out-of-plane conductivity of 1.06×10^{-5} S cm^{-1} at 40% RH, which increased to 1.21×10^{-2} S cm^{-1} at 90% RH. This significant improvement in the out-of-plane conductivity of Phy-3DGO suggests that the material retains superior proton-conducting properties even in the vertical direction, where proton transport is generally more challenging due to the layered structure of GO. The larger interlayer spacing introduced by phytic acid intercalation likely facilitates proton movement between the layers, leading to enhanced out-of-plane conductivity. At elevated
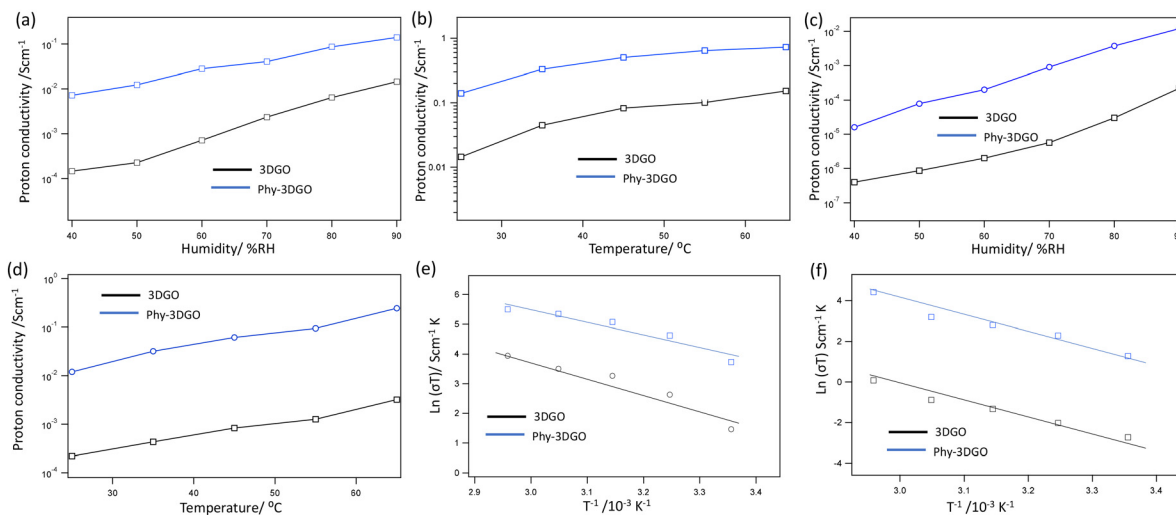
© 2025 The Author(s). Published by the Royal Society of Chemistry

RSC Appl. Interfaces, 2025, **2**, 734–740 | 737

Fig. 2 Proton conduction properties of 3DGO and Phy-3DGO. a) RH-dependent proton conductivity of 3DGO and Phy-3DGO in the in-plane direction at room temperature, b) temperature-dependent proton conductivity of 3DGO and Phy-3DGO at 90% RH in the in-plane direction, c) RH-dependent proton conductivity of 3DGO and Phy-3DGO in the out-of-plane direction at room temperature, d) temperature-dependent proton conductivity of 3DGO and Phy-3DGO at 90% RH in the out-of-plane direction, e) Arrhenius plot obtained from temperature-dependent proton conduction in the in-plane direction, and f) Arrhenius plot obtained from temperature-dependent proton conduction in the out-of-plane direction.

temperatures (Fig. 2d), the out-of-plane conductivity for 3DGO at 90% RH and 65 °C was 3.21×10^{-3} S cm^{-1}, while Phy-3DGO exhibited a much higher conductivity of 2.45×10^{-1} S cm^{-1}. This dramatic difference reinforces the superior proton conduction properties of Phy-3DGO, particularly under high humidity and temperature conditions, making it a highly promising material for proton-conducting applications, such as in fuel cells or proton exchange membranes.

The Arrhenius plots in Fig. 2e and f were used to calculate the activation energies for proton conduction in both materials for the in-plane and out-of-plane directions, respectively. The calculated activation energies were 0.31 eV for 3DGO and 0.19 eV for Phy-3DGO in the in-plane direction (Fig. 2e), with the lower activation energy for Phy-3DGO suggesting that it requires less energy for proton conduction, likely due to the enhanced proton transport pathways provided by the phytic acid. Furthermore, the low activation energy (<0.40 eV) indicates the proton transportation through the Grotthuss mechanism.[19] Similar to the in-plane results, the lower activation energy (0.37 eV for 3DGO and 0.28 eV for Phy-3DGO) in the out-of-plane indicates that proton transport is energetically more favorable in Phy-3DGO, further supporting the enhanced conductivity observed in the experimental data. The results clearly demonstrate that Phy-3DGO exhibits significantly enhanced
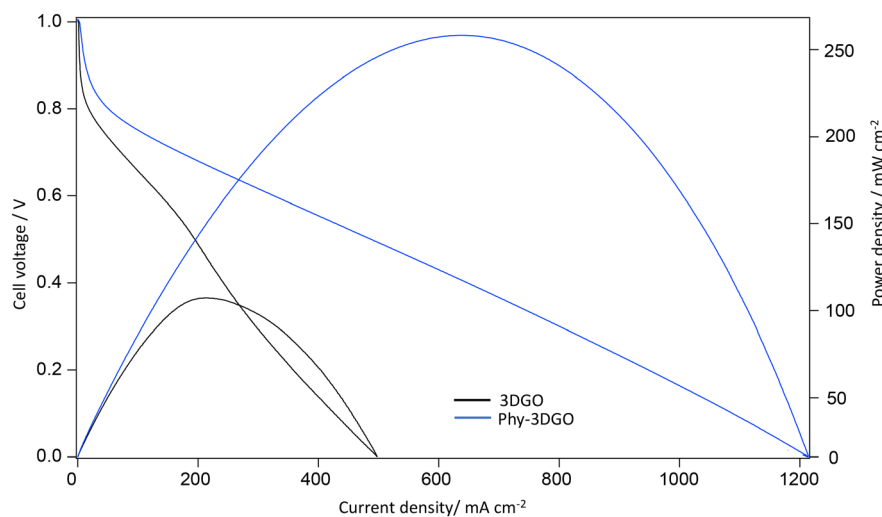

Fig. 3 The single-cell performance evaluation using the 3DGO membrane and Phy-3DGO as the proton conducting electrolyte. *I–V* curves and power densities for the 3DGO and Phy-3DGO membrane fuel cells.

proton conductivity compared to 3DGO, both in-plane and out-of-plane, under varying humidity and temperature conditions.

Furthermore, Phy-3DGO was assembled into a membrane electrode assembly (MEA) to evaluate its potential as an electrolyte in a practical fuel cell device. The performance was compared with that of pristine 3DGO. Single-cell performance testing was conducted at 30 °C and 100% RH. For Phy-3DGO, a high open-circuit voltage (OCV) of over 1.0 V at 30 °C was observed, indicating low fuel crossover and suitability for practical applications. The current–voltage ($I–V$) and current–power density curves are presented in Fig. 3. A maximum current density of 1210 mA cm^{-2} and a maximum power density (MPD) of 248.2 mW cm^{-2} were achieved using a 170 μm-thick Phy-3DGO film. In contrast, the pristine 3DGO membrane under identical conditions yielded an MPD of 98.1 mW cm^{-2} with a 113 μm-thick 3DGO film (Fig. 3).

In recent years, various strategies have been developed to enhance proton conductivity for practical applications as proton exchange membranes in fuel cells.[30–32] Phytic acid is an effective additive for enhancing the proton conductivity of GO due to its unique chemical structure and properties. The key reason lies in the presence of six phosphate groups in the phytic acid molecule, which provides abundant sites for proton donation and acceptance, facilitating efficient proton hopping *via* the Grotthuss mechanism. Particularly, phytic acid acts as a cross-linking agent for GO sheets. The phosphate groups in phytic acid can form covalent or non-covalent interactions with the hydroxyl and carboxyl groups on GO, creating a three-dimensional interconnected network. This cross-linking effect stabilizes the GO structure. Additionally, the ability of phytic acid to intercalate between the layers of GO increases the interlayer spacing, which was confirmed through the PXRD analysis with an enhanced interlayer distance. Furthermore, phytic acid is highly hydrophilic, which enhances the water retention capacity of the composite material. Since proton conduction is often dependent on the presence of water, this improved hydration further boosts proton transport across the material. Phytic acid also helps in dispersing GO sheets more effectively, preventing aggregation and maximizing the available surface area for proton conduction. This ensures a uniform distribution of conductive pathways, leading to higher proton conductivity. The interfacial interactions between 3DGO and phytic acid in Phy-3DGO are primarily driven by hydrogen bonding and electrostatic interactions. Phytic acid, with its multiple hydroxyl and phosphate groups, forms strong hydrogen bonds with the oxygen-containing functional groups on the GO surface. Additionally, the negatively charged phosphate groups of phytic acid interact electrostatically with positively charged regions on GO, such as protonated hydroxyl or carboxyl groups. These interactions facilitate the stable intercalation of phytic acid, increasing the interlayer distance of GO and creating expanded, hydrated pathways for proton conduction. This structural modification enhances the proton conductivity and fuel cell performance of phytic acid-intercalated 3DGO compared to that of pristine 3DGO. These attributes collectively make phytic acid an optimal choice for improving the proton conductivity of GO, making it highly suitable for applications in energy storage and conversion devices.

Conclusions

In summary, we have intercalated the phytic acid in the GO through a freeze-dried route. The interaction of phytic acid groups in 3DGO was confirmed through FTIR and PXRD analysis. The FTIR and XPS results confirmed the presence of phosphorus in the resulting Phy-3DGO. Furthermore, the intercalation of phytic acid into GO significantly enhances the interlayer distance and water uptake ability. These structural changes contribute to improved proton conductivity and fuel cell performance, making Phy-3DGO a superior material to pristine 3DGO. The current results indicate the potential of phytic acid intercalation in advancing the performance of graphene oxide-based proton exchange membranes in the fuel cell application.

Data availability

The data supporting this article have been included as part of the ESI.†

Author contributions

All authors checked the final version of the manuscript and agreed to submit it.

Conflicts of interest

There are no conflicts to declare.

Notes and references

1 M. S. Islam, Y. Shudo and S. Hayami, *Bull. Chem. Soc. Jpn.*, 2022, **95**, 1–25.

2 M. Fukuda, M. S. Islam, R. Shimizu, H. Nasser, N. N. Rabin, Y. Takahashi, Y. Sekine, L. F. Lindoy, T. Fukuda and T. Ikeda, *ACS Appl. Nano Mater.*, 2021, **4**, 11881–11887.

3 H. Takehira, M. S. Islam, M. R. Karim, Y. Shudo, R. Ohtani, L. F. Lindoy, T. Taniguchi, M. Osada and S. Hayami, *ChemistrySelect*, 2017, **2**, 6941–6944.

4 J. Yagyu, M. S. Islam, H. Yasutake, H. Hirayama, H. Zenno, A. Sugimoto, S. Takagi, Y. Sekine, S.-I. Ohira and S. Hayami, *Bull. Chem. Soc. Jpn.*, 2022, **95**, 862–870.

5 M. S. Islam, J. Yagyu, Y. Sekine, S. Sawa and S. Hayami, *Mater. Adv.*, 2022, **3**, 3418–3422.

6 M. S. Islam, M. R. Karim, S. Islam, J. Kim, N. N. Rabin, R. Ohtani, M. Nakamura, M. Koinuma and S. Hayami, *ChemistrySelect*, 2016, **1**, 6429–6433.

7 J. Kim, L. J. Cote and J. Huang, *Acc. Chem. Res.*, 2012, **45**, 1356.

© 2025 The Author(s). Published by the Royal Society of Chemistry

RSC Appl. Interfaces, 2025, **2**, 734–740 | 739

8 K. Wakata, M. R. Karim, M. S. Islam, R. Ohtani, M. Nakamura, M. Koinuma and S. Hayami, *Chem. – Asian J.*, 2017, **12**, 194–197.

9 M. Acik, C. Mattevi, C. Gong, G. Lee, K. Cho, M. Chhowalla and Y. J. Chabal, *ACS Nano*, 2010, **4**, 5861–5868.

10 Y. W. Zhu, S. Murali, W. W. Cai, X. S. Li, J. W. Suk, J. R. Potts and R. S. Ruoff, *Adv. Mater.*, 2010, **22**, 3906–3924.

11 U. Eberle, B. Müller and R. von Helmolt, *Energy Environ. Sci.*, 2012, **5**, 8780–8798.

12 Y. Wang, D. F. Ruiz Diaz, K. S. Chen, Z. Wang and X. C. Adroher, *Mater. Today*, 2020, **32**, 178–203.

13 R. K. A. M. Mallant, *J. Power Sources*, 2003, **118**, 424–429.

14 S. Akbari, M. T. Hamed Mosavian, F. Moosavi and A. Ahmadpour, *Composites, Part B*, 2019, **161**, 402–410.

15 J. H. Jung, J. H. Jeon, V. Sridhar and I. K. Oh, *Carbon*, 2011, **49**, 1279–1289.

16 H. Zarrin, D. Higgins, Y. Jun, Z. Shen and M. Fowler, *J. Phys. Chem. C*, 2011, **115**, 20774–20781.

17 B. A. Aragaw, W. N. Su, J. Rick and B. J. Hwang, *RSC Adv.*, 2013, **3**, 23212–23221.

18 M. R. Karim, K. Hatakeyama, T. Matsui, H. Takehira, T. Taniguchi, M. Koinuma, Y. Matsumoto, T. Akutagawa, T. Nakamura, S.-i. Noro, T. Yamada, H. Kitagawa and S. Hayami, *J. Am. Chem. Soc.*, 2013, **135**, 8097–8100.

19 K. Hatakeyama, M. R. Karim, C. Ogata, H. Tateishi, A. Funatsu, T. Taniguchi, M. Koinuma, S. Hayami and Y. Matsumoto, *Angew. Chem., Int. Ed.*, 2014, **53**, 6997–7000.

20 K. Wakata, M. S. Islam, M. R. Karim, K. Hatakeyama, N. N. Rabin, R. Ohtani, M. Nakamura, M. Koinuma and S. Hayami, *RSC Adv.*, 2017, **7**, 21901–21905.

21 W. Gao, G. Wu, M. T. Janicke, D. A. Cullen, R. Mukundan, J. K. Baldwin, E. L. Brosha, C. Galande, P. M. Ajayan, K. L. More, A. M. Dattelbaum and P. Zelenay, *Angew. Chem., Int. Ed.*, 2014, **53**, 3588–3593.

22 J. Lin, J. Dong, G. Zhou, W. Wu, Y. Liu, Y. Zhang and J. Wang, *J. Mater. Chem. A*, 2020, **8**, 10822–10830.

23 J. Wang, Y. Liu, J. Dang, G. Zhou, Y. Wang, Y. Zhang and L. Qu, *J. Membr. Sci.*, 2020, **602**, 117978.

24 B. Shi, H. Wu, J. Xhen, L. Cao, X. He, Y. Ma, Y. Li, J. Li, M. Xu, X. Mao, M. Qiu, H. Geng, P. Yang and Z. Jiang, *ACS Nano*, 2019, **13**, 10366–10375.

25 M. Fukuda, M. S. Islam, Y. Shudo, J. Yagyu, L. F. Lindoy and S. Hayami, *Chem. Commun.*, 2020, **56**, 4364–4367.

26 M. R. Karim, M. S. Islam, K. Hatakeyama, M. Nakamura, R. Ohtani, M. Koinuma and S. Hayami, *J. Phys. Chem. C*, 2016, **120**, 21976–21982.

27 J. Yagyu, M. S. Islam, Y. Shudo, M. Fukuda, H. Ushijima, J. Ohyama, S. Ida, L. F. Lindoy and S. Hayami, *ACS Appl. Energy Mater.*, 2021, **4**, 6296–6301.

28 M. A. Rahman, J. Yagyu, M. S. Islam, M. Fukuda, S. Wakamatsu, R. Tagawa, Z. Feng, Y. Sekine, J. Ohyama and S. Hayami, *ACS Appl. Nano Mater.*, 2023, **6**, 1707–1713.

29 M. Amine, F. Asafar, L. Bilali and M. Nadifiyine, *J. Chem.*, 2019, **2019**, 4675276.

30 J. Lin, J. Dang, G. Zhou, W. Wu, Y. Liu, Y. Zhang and J. Wang, *J. Mater. Chem. A*, 2020, **8**, 10822–10830.

31 J. Wang, J. Lin, Z. Zhou, Y. Zhang, Z. Yang and W. Wu, *J. Membr. Sci.*, 2021, **640**, 119818.

32 J. Wang, Y. Liu, J. Dang, G. Zhou, Y. Wang, Y. Zhang, L. Qu and W. Wu, *J. Membr. Sci.*, 2020, **602**, 117978.

© 2025 The Author(s). Published by the Royal Society of Chemistry